

MeshRipple: Structured Autoregressive Generation of Artist-Meshes

Junkai Lin¹ Hang Long¹ Huipeng Guo¹ Jielei Zhang¹ Jiayi Yang¹ Tianle Guo¹ Yang Yang¹
 Jianwen Li² Wenxiao Zhang² Matthias Nießner³ Wei Yang^{1,†}

¹ Huazhong University of Science and Technology ² Independent Researcher

³ Technical University of Munich

<https://maymhappy.github.io/MeshRipple/>



Figure 1. **Gallery of results generated by MeshRipple.** Our method handles diverse mesh styles and topologies, producing artist-style meshes with optimized topology (airplane, train, totem) as well as dense smooth-surface meshes (bears, unicorn, dinosaur), all with coherent geometry and high-fidelity details.

Abstract

*Meshes serve as a primary representation for 3D assets. Autoregressive mesh generators serialize faces into sequences and train on truncated segments with sliding-window inference to cope with memory limits. However, this mismatch breaks long-range geometric dependencies, producing holes and fragmented components. To address this critical limitation, we introduce **MeshRipple**, which expands a mesh outward from an active generation frontier,*

akin to a ripple on a surface. MeshRipple rests on three key innovations: a frontier-aware BFS tokenization that aligns the generation order with surface topology; an expansive prediction strategy that maintains coherent, connected surface growth; and a sparse-attention global memory that provides an effectively unbounded receptive field to resolve long-range topological dependencies. This integrated design enables MeshRipple to generate meshes with high surface fidelity and topological completeness, outperforming strong recent baselines.

† corresponding author: weiyangcs@hust.edu.cn

1. Introduction

Meshes are the native representation for high-quality 3D assets in film, game, and product design pipelines, and are supported by virtually all graphics tools and hardware. Directly generating editable, simulation-ready meshes can thus substantially reduce artist workload and accelerate industrial content creation. One approach is to generate continuous fields from latent codes with diffusion models and then extract surfaces via marching cubes [23, 24, 43, 68, 69, 77, 80, 83]. While effective for geometry, this pipeline offers limited control over topology: marching cubes tends to produce overly dense, irregular, and non-artist-friendly meshes that require extensive post-processing.

Recent work instead employs autoregressive (AR) models to directly synthesize meshes with artist-like topology, often conditioned on input geometry such as point clouds. These methods tokenize meshes into sequences and learn a next-token distribution that respects mesh connectivity, leading to more structured and production-ready outputs. However, representing large, detailed meshes in sequence form inevitably yields excessively long token streams. To make AR training tractable, state-of-the-art approaches adopt a truncated-training strategy: the sequence is partitioned into fixed-length context windows; each window is trained independently; and, at inference, a rolling KV cache is used to approximate longer-range context [28, 29, 82]. Yet existing tokenization schemes, including coordinate-based orderings [4, 28, 38, 47], depth-first expansion [27, 54], and block-/patch-based encodings [54, 65, 82], do not guarantee that the relevant elements fall within the truncated window. As a result, the model is frequently forced to predict connectivity without seeing the correct local neighborhood, leading to broken surfaces and fragmented components. Rolling the KV cache at inference time cannot fundamentally fix this issue, since the model was never consistently trained with the true context. Recent advances, such as DeepMesh [82], MeshRFT [29], and QuadGPT [28], improve performance via preference-based fine-tuning with reinforcement learning. While these approaches enhance topological quality and style alignment, they do not fully resolve connectivity errors.

In this work, we introduce **MeshRipple**, a topology-aligned autoregressive framework for generating large, artist-friendly triangle meshes with high structural fidelity. The core component is Ripple Tokenization (RT), which couples a breadth-first face ordering with an explicit, dynamically maintained frontier: we traverse faces in half-edge based BFS order; at each step we maintain the set of faces that bound at least one unvisited neighbor (the frontier); and for every newly added face we record a root pointer to the frontier face from which it grows. By construction, the structurally relevant tokens for the next face prediction occupies the most recent portion of the sequence.

Hence, a truncated window that covers the tail segment containing the frontier reliably includes the local context required for the next face, directly mitigating the topology-context mismatch that limits prior tokenizations.

Building on RT, we design an autoregressive transformer tailored for structured mesh growth. A compact hourglass backbone first compresses fine-grained vertex tokens into per-face embeddings. Upon which, at each step, the model jointly predicts the the grown face attached to the current root, and the next root to expand, constraining generation to expand a coherent surface rather than freely sampling incompatible triangles. To incorporate longer-range cues (e.g., symmetry and repetition) without prohibitive memory, we introduce Native Sparse Contextual Attention (NSCA): a causal, sparsified cross attention mechanism that queries a compressed summary of the full mesh history and selectively retrieves detailed relevant tokens. NSCA complements the local truncated window while keeping computation and memory bounded. Through this structure-aware design, MeshRipple aligns tokenization, truncated training, and autoregressive inference. The result is a substantial reduction in broken surfaces and artifacts, enabling high-face-count mesh generation at scale (see Figure 1).

In summary, our contributions are three-fold:

- **Ripple Tokenization.** A topology-aligned face traversal with an explicit frontier that concentrates the relevant tokens into the tail of the sequence, aligning tokenization with truncated autoregressive training.
- **Expansive Prediction Strategy.** A decoding scheme that jointly predicts the root and the attached face, enforcing face frontier connectivity.
- **Native Sparse Contextual Attention (NSCA).** A causal sparse attention module that retrieves long-range mesh cues, supporting scale-up generation of meshes.

2. Related Work

3D Shape Generation. Early work on 3D generation, constrained by scarce 3D data, largely follows two strategies. One line adopts SDS-based optimization from image diffusion models [3, 7, 21, 25, 36, 40, 42, 51, 53, 57, 60, 61, 75], while another predicts multi-view images and then reconstructs 3D geometry from them [8, 16, 26, 30–32, 34, 41, 45, 46, 56, 58, 66, 72, 74, 81]. LRM [15] then introduces a transformer-based reconstructor that predicts a NeRF representation [37] from a single image, and subsequent work [20, 48, 52, 59, 63, 70, 71, 78, 79, 84, 85] improves this paradigm with multi-view supervision and alternative 3D parameterizations such as 3D Gaussians [18]. In parallel, early 3D-native diffusion models [2, 13, 17, 33, 39] operate directly on point clouds, but are limited by dataset scale and generalization. 3DShape2VecSet [77] instead encodes point clouds into a latent set and learns a generative distribution in this space, and CLAY [80] demonstrates

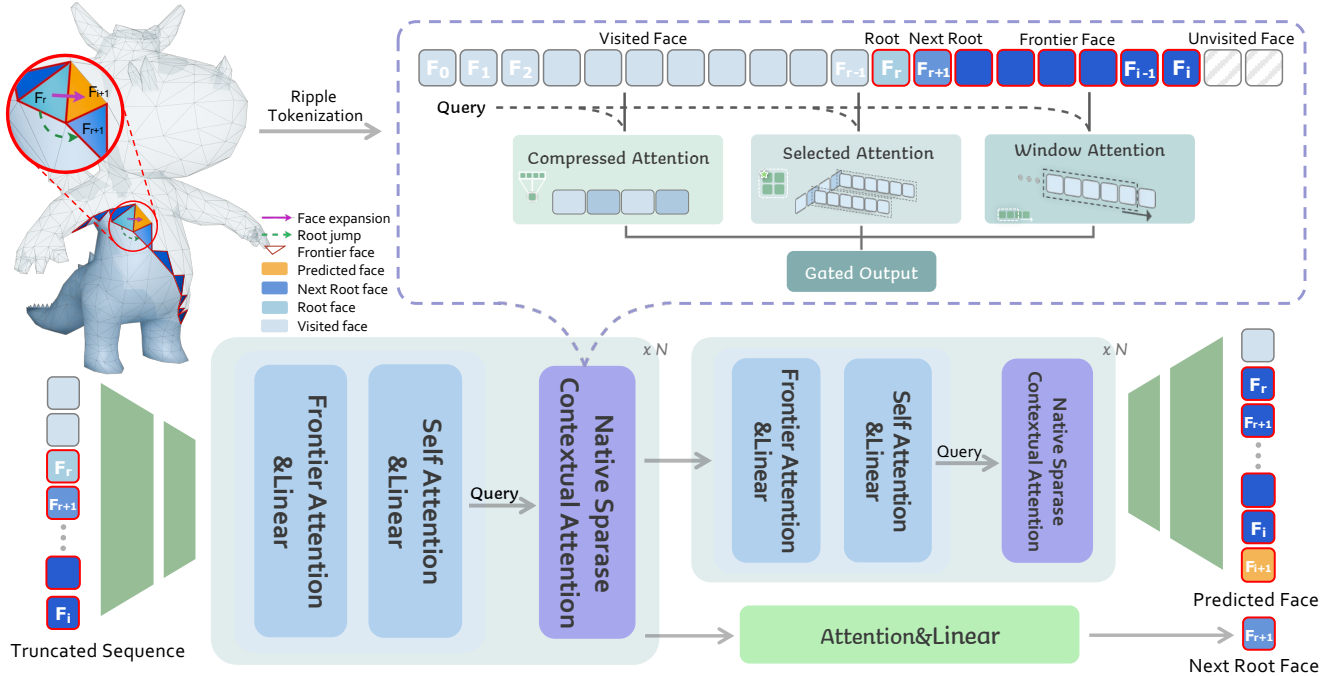


Figure 2. **Overview of MeshRipple.** The input mesh is first serialized into a token sequence via **Ripple Tokenization**, which is then truncated into fixed-length segments as input to a structured autoregressive model. The model employs hourglass layers at both ends to convert between vertex and face tokens. The core consists of a stack of $2 \times N$ identical blocks, each comprising a **Frontier-Attention** layer, a self-attention layer, a cross-attention layer for point-cloud conditioning (omitted for clarity), and a **Native Sparse Contextual Attention** layer that attends to the full mesh sequence under a causal mask. The middle hidden states are additionally fed into a lightweight head to predict the next root face to expand.

that this paradigm can be scaled up effectively. Subsequent methods [9, 22, 23, 67, 73, 83] further enrich the latent representation with textures and normals, or refine geometric detail via normal supervision. Trellis [69] adopts a more structured latent space based on sparse voxels, while Direct3D-S2 [69] and Sparc3D [24] extend this idea using multi-resolution latents or higher-resolution voxel decoders. The aforementioned methods generate 3D assets in implicit or volumetric form and only obtain meshes via post-hoc extraction (e.g., Marching Cubes [35]). The resulting faces are often overly dense and require significant post-processing.

Mesh Tokenization and Autoregressive Generation. Autoregressive models that generate meshes directly have attracted growing interest. PolyGen [38] predicts vertices and edges separately, while MeshGPT [47] pioneers the combination of a VQ-VAE [55] with an autoregressive transformer for mesh synthesis; later works [4, 5, 62, 64] explore alternative architectures and conditional settings. In parallel, the community has rapidly shifted toward explicit mesh quantization and tokenization: MeshAnythingv2 [6] introduces Adjacent Mesh Tokenization (AMT), EdgeRunner [54] derives a sequence via an EdgeBreaker-style traversal [44], BPT [65] adopts a patchified, blockwise strategy, and Mesh Silksong [49] tokenizes edges with a BFS-style traversal. These tokenizers primarily aim to maximize com-

pression to alleviate memory constraints. MeshTron [14] instead operates directly on vertex coordinates and employs an hourglass architecture for compression. DeepMesh [82] and MeshRFT [29] introduce reinforced fine-tuning to improve topology quality, and QuadGPT [28] extends to quadrilateral meshes. Despite this progress, these approaches still suffer from broken surfaces.

3. Method

Our framework aims to generate large, structurally coherent meshes under truncated autoregressive (AR) training. It consists of two key components: (i) **Ripple Tokenization**, which couples a breadth-first face ordering with an explicit dynamically maintained frontier, such that the structurally relevant context for the next face prediction is concentrated near the tail of the sequence; and (ii) **an structured autoregressive transformer** with frontier attention and a lightweight context attention that jointly predicts the next face attached to current root face, and the subsequent root face on the frontier to expand.

3.1. Ripple Tokenization

We conduct a half-edge based breadth-first traversal of faces with an explicit, dynamically maintained frontier queue. At

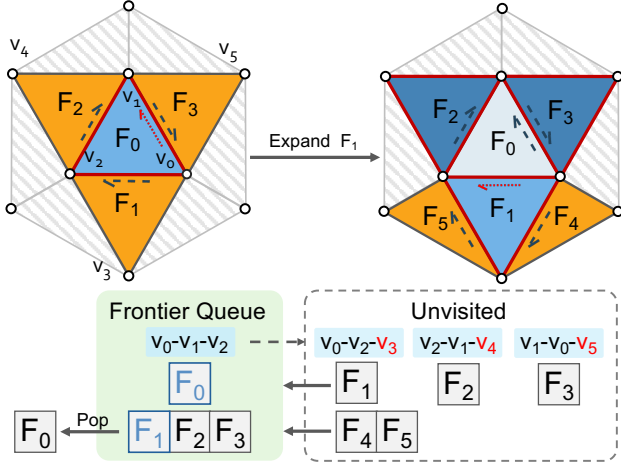


Figure 3. **Illustration of Ripple Tokenization.** At each step, the current root face expands following the counterclockwise half-edge order. Faces that still have unvisited neighbors remain in the FIFO frontier queue; once all neighbors are visited, the face is popped from the queue.

each step, we grow new faces from a set of frontier faces that bound the already generated region. This construction ensures that, for any next face to be predicted, its incident neighborhood lies within the most recent portion of the sequence, making truncated training well-aligned with mesh topology. Given a triangle mesh $\mathcal{M} = (\mathcal{V}, \mathcal{F})$, we follow standard practice as in [14, 82] and discretize vertex coordinates, by normalizing \mathcal{V} into a canonical bounding box and uniformly quantize each coordinate. Each face $\mathbf{F}_i \in \mathcal{F}$ is represented by three quantized vertices, $F_i = [\mathbf{v}_0^i, \mathbf{v}_1^i, \mathbf{v}_2^i]$. To support consistent traversal and ensure the consistency of generated face normals, we orient each face in a counterclockwise order with respect to its outward normal, and derive its three directed half-edges: $(\mathbf{v}_0^i \rightarrow \mathbf{v}_1^i)$, $(\mathbf{v}_1^i \rightarrow \mathbf{v}_2^i)$, $(\mathbf{v}_2^i \rightarrow \mathbf{v}_0^i)$. Therefore, two faces are considered adjacent if they share a pair of opposite half-edges (a half-edge and its twin).

3.1.1. BFS Traversal

Starting from an initial seed face \mathbf{F}_s , we perform a breadth-first ordering over faces using the half-edge connectivity. For a face, we look at its three directed half-edges in their fixed (e.g., counterclockwise) order. For each half-edge, if there is an adjacent face across its twin that has not been visited, we mark this neighbor as visited, append it to the output sequence \mathcal{S} , and schedule it to be expanded later. In this way, new faces are discovered and inserted into the sequence following the local half-edge order of their root face, giving a deterministic, topology-respecting BFS ordering.

Non-manifoldness. Our method inherently handles non-manifold edges, i.e., when an edge is incident to more than two faces, our half-edge structure records all corresponding twins and each incident face is simply treated as a valid

neighbor. For non-manifold vertices, our algorithm naturally divides them into separate disconnected components.

Disconnected Components. For meshes with multiple connected components, we process each component independently with the BFS procedure. Between components, we insert a special control token \mathbf{N} into \mathcal{S} .

3.1.2. Frontier Queue and Root-Face Registration

To make the traversal explicitly compatible with truncated AR training, we maintain a FIFO frontier queue \mathcal{B}_i for each face \mathbf{F}_i . Concretely during the BFS traversal, when a face \mathbf{F}_i is appended to \mathcal{S} , we record a root index r_i : $r_i \in \{1, \dots, |\mathcal{S}|\}$, indicating from which face $\mathbf{F}_{r_i} \in \mathcal{B}$ the new face \mathbf{F}_i is grown (i.e., which shared edge induces its attachment). And if all neighbors of \mathbf{F}_{r_i} have been visited, we remove it from \mathcal{B}_i . Then we add \mathbf{F}_i into \mathcal{B}_i , it forms a new frontier \mathcal{B}_{i+1} for \mathbf{F}_{i+1} . Hence, for each face \mathbf{F}_i in mesh sequence \mathcal{S} , we have recorded:

$$\mathbf{F}_i \leftarrow \{r_i, \mathcal{B}_i\} \quad (1)$$

Notice that \mathbf{F}_{r_i} is always the first face in \mathcal{B}_i due to BFS. This design ensures that the relevant context (the active frontier) is always located near the end of the sequence. And a truncated window that covers the last L tokens thus contains the necessary context to predict the next face (see Figure 3 for detailed explanation). Also, the root index r_i restricts autoregressive sampling to expand from valid boundary locations, substantially reducing topological ambiguities and broken surfaces. Existing tokenization schemes either follow a coordinate-ordered traversal [4, 14, 47], depth-frist expansion [27, 54] or a patch-based encoding [65, 82], important tokens can easily fall outside the truncated input sequence. The most related work to ours is the concurrent work Mesh Silksong [49], which also adopts a breadth-first traversal. However, we differ fundamentally as Mesh Silksong tokenize both vertices and edges, resulting in an excessively large vocabulary, and requires preprocessing for non-manifoldness. In contrast, our method is more flexible: it explicitly maintains a frontier set of boundary faces, simplifies the prediction space, and naturally extends to non-manifold configurations.

3.2. Structured Autoregressive Model

Given a mesh encoded by Ripple Tokenization, our goal is to autoregressively generate faces in a way that respects the frontier-based growth process while compatible with truncated training. To this end, we design a structured autoregressive transformer equipped with three key components: a **Frontier Attention** mechanism that emphasizes structurally relevant frontier faces, a **Native Sparse Contextual Attention** (NSCA) module that injects long-range mesh context under strict memory constraints, and an **Expansive Prediction** scheme that jointly predicts the new face

grown from the current root and the next root face to expand. Please see Figure 2 for the detailed framework. Starting from the quantized coordinate sequence \mathcal{S} , we adopt an outer hourglass-style transformer to progressively merge: coordinate-level tokens into vertex-level embeddings, and finally into face-level tokens, where each token corresponds to one face. Subsequent conditioning, frontier and contextual attentions are applied at the face-token level.

Truncated Training High-poly meshes induce long face sequences. We follow the standard truncated training regime as in MeshTron [14] and DeepMesh [82] and partition the mesh sequence into fixed-size windows, with padding applied to insufficient-length segments.

3.2.1. Frontier Attention

For each face \mathbf{F}_i , let \mathcal{B}_i denote the FIFO frontier queue constructed during tokenization. Faces in \mathcal{B}_i are precisely those from which valid growth can occur. To emphasize this structure, we introduce a frontier attention layer. It uses standard multi-head attention over the windowed input tokens, but with a mask that restricts attention toward the current frontier: for the query at position i , only tokens corresponding to faces in \mathcal{B}_i (and not beyond i) are assigned non-negative logits; all others are masked out.

$$\mathbf{M}_{i,j}^b = \begin{cases} 0, & \mathbf{F}_j \in \mathcal{B}_i \text{ and } j \leq i \\ -\text{Inf}, & \text{otherwise} \end{cases} \quad (2)$$

This encourages the model to primarily from the active growth boundary when predicting the next face, and route gradients to the subset of tokens that are structurally responsible for connectivity.

3.2.2. Native Sparse Contextual Attention

While frontier attention provides accurate local structure, many meshes exhibit long-range patterns. Conventional sliding-window inference approximates this with KV rolling caches suffers training-inference inconsistency problem. To address, we propose NSCA, which offers causal, memory-efficient access to the full mesh history.

For the given full mesh sequence \mathcal{S} , we first obtain coordinate-level embeddings, aggregate them into vertex-level embeddings, and finally to a per-face token by concatenating along the channel dimension, which is finally projected by a small MLP to a pre-defined hidden dimension. We partition the full face sequence into non-overlapping blocks. Note that the query tokens in the main model are taken from the truncated window, whereas the keys and values for NSCA are computed from the full sequence, so their lengths differ. To ensure causal consistency, we construct masks at both the block and token levels: for any block that contains tokens positioned after the current step, we assign its entire block in the mask with $-\text{inf}$, so it cannot be attended to when predicting the current token. Following the original

DeepSeek’s Native Sparse Attention [76], each valid block is mapped to a single compressed key–value pair. Using the hidden state of the main autoregressive model as query, we compute an importance score for each compressed block token and select the top- k blocks, for which we then retrieve the original (uncompressed) keys and values. In parallel, we maintain a standard local window of each token. A block-level causal mask is applied to all compressed and selected tokens, while a token-level causal mask is used for the local window. Finally, a lightweight router learns to weight and fuse three sources—the compressed block tokens, the detailed tokens from the top- k selected blocks, and the local window—and the resulting mixture is used as the contextual memory attended by the query.

3.2.3. Expansive Prediction

Unlike prior autoregressive models that only predict the next face token, we adopt an *expansive prediction* strategy: at each step, the model jointly predicts **the new face** grown from the current root, and **the next root face** to expand on the frontier. Concretely, we attach an additional root prediction head to middle of the network. Instead of predicting the next root face token directly, we let the model predict how many positions to move along the FIFO frontier from the current root to obtain the next root. Formally, let \mathbf{F}_i and \mathbf{F}_{i+1} are two adjacent faces in input sequence, and let r_i and r_{i+1} be their root face indices respectively. We define the offset steps as $\Delta_{i+1} = r_{i+1} - r_i$. Notice $\Delta_{i+1} = 0$ if \mathbf{F}_i and \mathbf{F}_{i+1} share the same root.

Training. A lightweight pointer head attends over the middle layer hidden states to produce $p_\theta(\Delta_{i+1})$, and the root loss is a standard cross-entropy

$$\mathcal{L}_{\text{root}} = - \sum_i \log p_\theta(\Delta_{i+1} | \mathbf{F}_t, t \leq i). \quad (3)$$

The overall training objective combines next root prediction loss and the standard next face prediction loss.

Inference. For inference, at each step we maintain a dynamic FIFO frontier queue \mathcal{B} , the current generated mesh sequence, and the current root face \mathbf{F}_r . To predict the next face, we enforce structural consistency by masking out all candidate faces that do not attach to \mathbf{F}_r , and then choose the final prediction \mathbf{F}^* from the remaining candidates using sampling-based decoding. We append \mathbf{F}^* to the full mesh sequence (used by NSCA) and to the autoregressive input, and update the frontier queue by adding \mathbf{F}^* . Meanwhile, the root pointer head predicts Δ , which selects the next root face \mathbf{F}'_r by moving forward Δ steps on the frontier. For the **N** token, we simply lift the connectivity constraint. We then update the root face \mathbf{F}_r to \mathbf{F}'_r , pop out all faces before \mathbf{F}'_r from \mathcal{B} . The frontier attention mask and causal attention mask for NSCA are updated accordingly, and conduct the next round prediction.

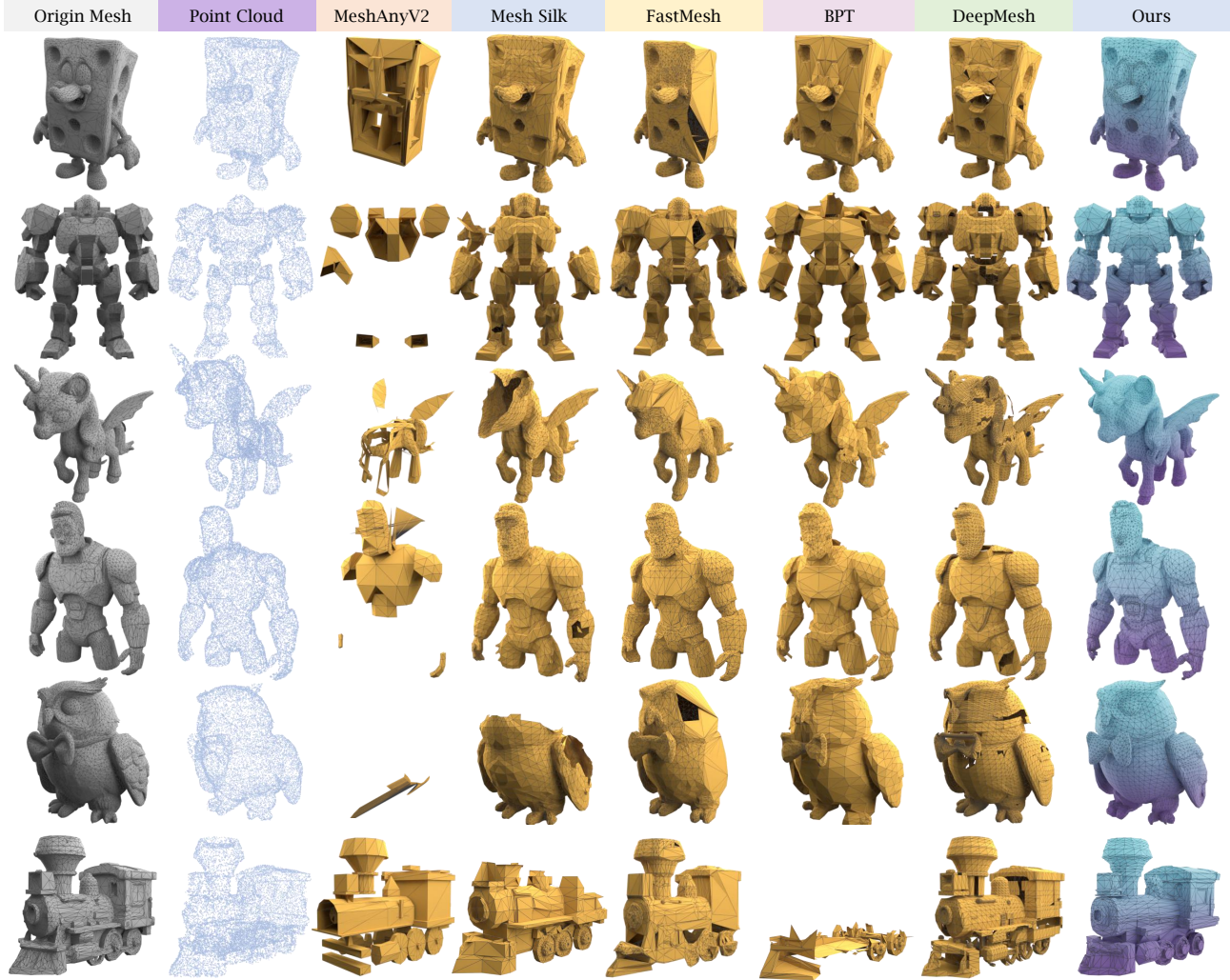


Figure 4. **Qualitative comparison of point cloud-conditioned generation between MeshRipple and baselines.** Baselines inevitably produce broken surfaces and holes, whereas MeshRipple yields more complete and coherent geometries.

4. Experiments

Datasets. We construct our dataset from Objaverse-XL [10], G-Objaverse [86], ShapeNet [1], Toys4K [50], and 3D-FUTURE [12]. We discard meshes with more than 20k or fewer than 500 faces, excessive discretization artifacts (over-aggressive vertex merging), more than 20 connected components, or an intersection ratio above 10, yielding roughly 300k meshes. For artist-mesh evaluation, we hold out 300 meshes from G-Objaverse and 50 each from Toys4K and ShapeNet. For dense-mesh evaluation, we generate 500 meshes using Trellis [69].

Implementation Details. The architecture follows a [4, 4, 9] Hourglass configuration with an embedding dimension of 1024, a 100-class next-root prediction head, and vertex quantization into 256 bins. For context injection, we use a 256-dimensional embedding that is concatenated along the channel dimension. For each mesh, we sample 40,960

points and randomly select 16,384 points as the condition. These point clouds are encoded into latent features by a Michelangelo encoder, which are then injected via cross-attention. We set the maximum mesh length to 20k faces, and the input sequence 1k faces. We train our model with AdamW optimizer, using a cosine learning rate schedule decays from 1×10^{-4} to 1×10^{-5} with weight decay 0.1. Training takes 16 days on 16 NVIDIA A800 GPUs.

4.1. Quantitative Analysis

We quantitatively compare our method with MeshAnythingv2 [6], BPT [65], FastMesh [19], Mesh Silksong [49], and DeepMesh [82] on two benchmarks: artist meshes and dense meshes. For fair evaluation, we uniformly sample 1,024 points from each generated mesh and its ground-truth counterpart, and report Chamfer Distance (CD), Hausdorff Distance (HD), and Normal Consistency (NC). As sum-

Table 1. **Quantitative comparison on Dense-Mesh and Artist-Mesh datasets.** We scale CD by 10^3 . The best result is highlighted in **bold**, and the second-best is underlined.

Dataset	Method	CD(↓)	HD(↓)	NC(↑)
Dense Mesh	MeshAnythingV2	109.64	0.2314	-0.0096
	BPT	60.19	0.1089	<u>0.6066</u>
	FastMesh	64.62	0.1155	0.0002
	Mesh SilkSong	61.99	0.1435	0.5529
	DeepMesh	<u>50.27</u>	0.0893	0.6025
	Ours	48.73	<u>0.1057</u>	0.6280
Artist Mesh	MeshAnythingV2	68.11	0.1433	-0.0504
	BPT	54.78	0.1014	<u>0.5084</u>
	FastMesh	<u>47.26</u>	<u>0.0972</u>	0.0106
	Mesh SilkSong	49.72	0.1019	0.4709
	DeepMesh	51.11	0.1023	0.3174
	Ours	46.68	0.0938	0.5166

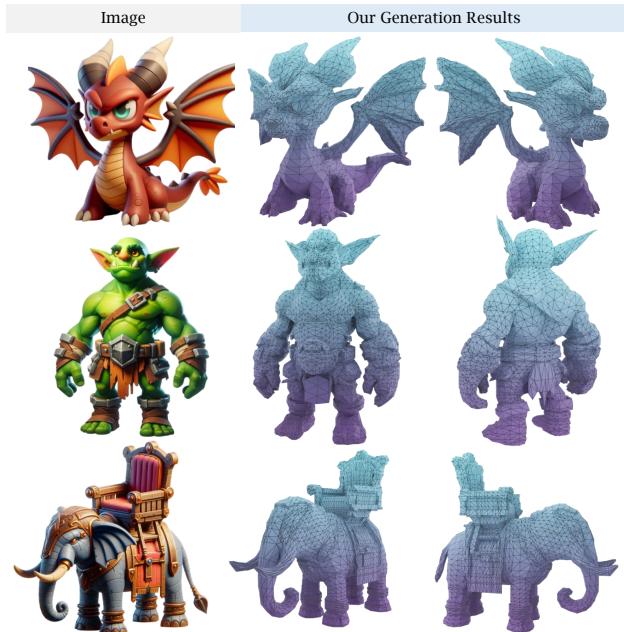


Figure 5. **Image-conditioned generation results.** Our method can generate high-fidelity meshes aligned with the input images.

marized in Table 1, our method achieves the best overall scores on the artist-mesh benchmark and performs competitively with DeepMesh on dense meshes, despite substantially lower compute: DeepMesh is pre-trained on 128 NVIDIA A100 GPUs for 4 days plus DPO post-training, whereas our model is trained on 16 A800 GPUs for 16 days.

4.2. Qualitative Analysis

Point-cloud Conditioned. We evaluate point cloud conditioned generation against five recent open-source baselines: MeshAnythingv2, BPT, FastMesh, Mesh Silksong, and DeepMesh. As shown in Figure 4, competing meth-

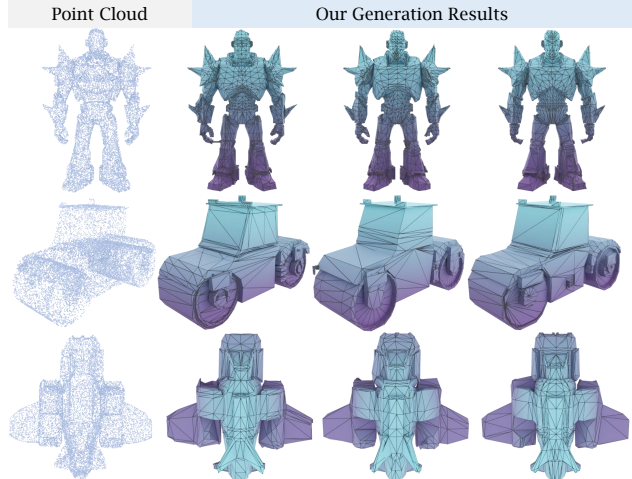


Figure 6. **Diversity of generations.** MeshRipple can generate meshes with diverse topologies given the same point cloud.

ods often miss fine topological structures and exhibit holes or fragmented geometry, whereas our meshes preserve both detail and global coherence. Our results are simultaneously more intricate than those of MeshAnything v2, BPT, FastMesh, and Mesh Silksong, and more structurally stable than those of DeepMesh. We attribute these gains to our topology-aware architecture, which couples global context modeling and point-cloud conditioning with an improved BFS expansion scheme based on a frontier mask.

Image Conditioned. For image conditioned generation, we adopt a two-stage pipeline. We first use TRELIS [69] to synthesize a 3D mesh from the input image, then extract a point cloud from this mesh to condition our point cloud-based generator. Representative high-quality results are shown in Figure 5.

Diversity. We assess the stochasticity of our generator by sampling multiple meshes from the same point-cloud input. As shown in Figure 6, the model produces a diverse set of plausible outputs while consistently preserving the underlying structure, demonstrating its ability to achieve both variation and high-fidelity synthesis.

Table 2. **Ablations of our design choices.** Best results shown in **bold**, second-best is underlined.

Method	CD		HD	
	Value ↓	Δ	Value ↓	Δ
Full Model (Ours)	<u>52.67</u>	-	<u>0.1058</u>	-
w/o Frontier Mask	54.79	+2.12	0.1199	+0.0141
w/o Context Injection	60.56	+7.89	0.1176	+0.0118
w/o Non-manifold	57.75	+5.08	0.1193	+0.0135
w/o NSCA	52.43	-0.24	0.1025	-0.0033
w/o Root Constraint	65.08	+12.41	0.1180	+0.0122

Scene Generation on 3D-FRONT. Our method supports

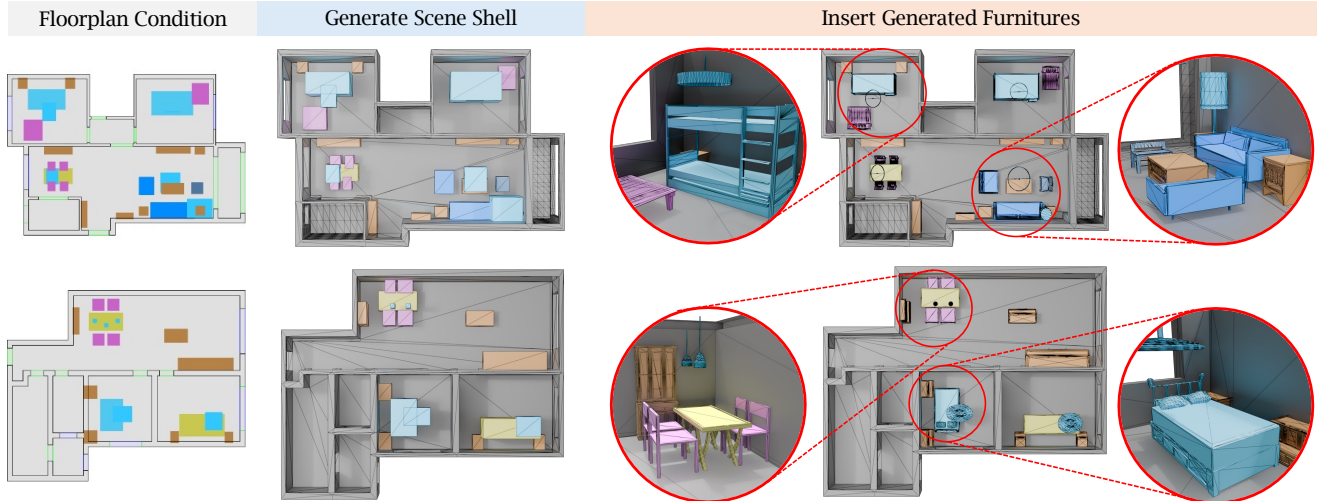


Figure 7. **Scene generation results.** MeshRipple supports topology variations, non-manifold geometres, and multi-component assemblies. We demonstrate this through progressive scene generation. Trained on 3D-FRONT, we first generate a room shell from a floorplan image, and predict category-labeled bounding-box placeholders for furniture; we then generate and insert each furniture mesh independently.

diverse frontier configurations arising from topology variation, non-manifold geometry, and multi-component assemblies. To demonstrate, we train on 3D-FRONT [11], which features varied topologies and component configurations. We replace each furniture instance with a category-labeled bounding-box placeholder to enable progressive prediction. We replace the component segment control token **N** with semantic tokens **CABINET**, **BED**, **CHAIR**, **TABLE**, **SOFA**, **STOOL**, and **LAMP**. At test time, we first generate a room shell from a floorplan and predict category-labeled bounding-box placeholders; we then generate each furniture mesh independently with MeshRipple, finetuned with ShapeNet, and place it into the corresponding location. High-quality results are shown in Figure 7.

Table 3. **Ablation on root prediction strategies.** We compare predicting absolute coordinates versus index offset.

Method	MMD ($\times 10^3$) \downarrow	1-NAA \downarrow	COV \uparrow
Coordinates	19.26	71.71	47.56
Index Offset	15.26	50.73	58.29

4.3. Ablation Study

Modules. We conduct ablation studies to quantify the effect of each proposed component. Specifically, we remove the frontier mask, context injection, the NSCA module, non-manifold encoding, and expansive reasoning in turn, and evaluate on 5k-face meshes with a validation subset of 128 meshes. Performance of CD and HD is shown in Table 2. The use of full context without NSCA achieves the best performance, while NSCA significant saves memory and time with minor performance drop.

Root Prediction. We further ablate the next-root prediction

Table 4. Memory (GB) and runtime (s) comparison w/o NSCA. Each configuration is evaluated and averaged over 128 iterations. Context and window sizes are measured in number of faces.

Total Faces	Window	NSCA		w/o NSCA	
		Time	Mem	Time	Mem
5K	1K	0.253	24.65	0.180	27.68
10K	1K	0.252	24.72	0.199	28.50
20K	2K	0.398	30.16	0.419	38.15
50K	5K	1.229	48.46	OOM	
100K	5K	1.275	49.19	OOM	

schemes: directly predict vertex coordinates versus predicting a relative offset step, as shown in Table 3.

Resources w/o NSCA. Table 7 compares the computational resource consumption with and without NSCA across various configurations. We set the NSCA kernel size to 32, sliding stride to 16, compression block size to 64, and select top 16 blocks.

5. Conclusion

We introduce **MeshRipple**, a structured autoregressive framework for artist-mesh generation with a frontier-aware BFS tokenization, an expansive prediction scheme, and a lightweight sparse contextual attention. It’s compatible with truncated training and produces complete, high-quality meshes, outperforming strong recent baselines.

Limitations and future work. Substantial label noise or extreme configurations can degrade our model’s performance. We plan to increase coordinate quantization resolution and scale to meshes with up to 100K faces, extend the framework to quad meshes, and merge our model with RL-based preference tuning.

References

- [1] Angel X Chang, Thomas Funkhouser, Leonidas Guibas, Pat Hanrahan, Qixing Huang, Zimo Li, Silvio Savarese, Manolis Savva, Shuran Song, Hao Su, et al. Shapenet: An information-rich 3d model repository. *arXiv preprint arXiv:1512.03012*, 2015. 6
- [2] Jen-Hao Rick Chang, Yuyang Wang, Miguel Angel Bautista Martin, Jiatao Gu, Xiaoming Zhao, Josh Susskind, and Oncel Tuzel. 3d shape tokenization via latent flow matching. *arXiv preprint arXiv:2412.15618*, 2024. 2
- [3] Rui Chen, Yongwei Chen, Ningxin Jiao, and Kui Jia. Fantasia3d: Disentangling geometry and appearance for high-quality text-to-3d content creation. In *IEEE/CVF International Conference on Computer Vision, ICCV 2023, Paris, France, October 1-6, 2023*, pages 22189–22199. IEEE, 2023. 2
- [4] Sijin Chen, Xin Chen, Anqi Pang, Xianfang Zeng, Wei Cheng, Yijun Fu, Fukun Yin, Billzb Wang, Jingyi Yu, Gang Yu, et al. Meshxl: Neural coordinate field for generative 3d foundation models. *Advances in Neural Information Processing Systems*, 37:97141–97166, 2024. 2, 3, 4
- [5] Yiwen Chen, Tong He, Di Huang, Weicai Ye, Sijin Chen, Jiaxiang Tang, Zhongang Cai, Lei Yang, Gang Yu, Guosheng Lin, and Chi Zhang. Meshanything: Artist-created mesh generation with autoregressive transformers. In *The Thirteenth International Conference on Learning Representations, ICLR 2025, Singapore, April 24-28, 2025*. OpenReview.net, 2025. 3
- [6] Yiwen Chen, Yikai Wang, Yihao Luo, Zhengyi Wang, Zilong Chen, Jun Zhu, Chi Zhang, and Guosheng Lin. Meshanything v2: Artist-created mesh generation with adjacent mesh tokenization. In *Proceedings of the IEEE/CVF International Conference on Computer Vision*, pages 13922–13931, 2025. 3, 6
- [7] Zilong Chen, Feng Wang, Yikai Wang, and Huaping Liu. Text-to-3d using gaussian splatting. In *IEEE/CVF Conference on Computer Vision and Pattern Recognition, CVPR 2024, Seattle, WA, USA, June 16-22, 2024*, pages 21401–21412. IEEE, 2024. 2
- [8] Zilong Chen, Yikai Wang, Feng Wang, Zhengyi Wang, and Huaping Liu. V3d: Video diffusion models are effective 3d generators. *arXiv preprint arXiv:2403.06738*, 2024. 2
- [9] Zhaoxi Chen, Jiaxiang Tang, Yuhao Dong, Ziang Cao, Fangzhou Hong, Yushi Lan, Tengfei Wang, Haozhe Xie, Tong Wu, Shunsuke Saito, Liang Pan, Dahua Lin, and Ziwei Liu. 3dtopia-xl: Scaling high-quality 3d asset generation via primitive diffusion. In *IEEE/CVF Conference on Computer Vision and Pattern Recognition, CVPR 2025, Nashville, TN, USA, June 11-15, 2025*, pages 26576–26586. Computer Vision Foundation / IEEE, 2025. 3
- [10] Matt Deitke, Ruoshi Liu, Matthew Wallingford, Huong Ngo, Oscar Michel, Aditya Kusupati, Alan Fan, Christian Laforte, Vikram Voleti, Samir Yitzhak Gadre, et al. Objaverse-xl: A universe of 10m+ 3d objects. *Advances in Neural Information Processing Systems*, 36:35799–35813, 2023. 6
- [11] Huan Fu, Bowen Cai, Lin Gao, Lingxiao Zhang, Jiaming Wang, Cao Li, Qixun Zeng, Chengyue Sun, Rongfei Jia, Binqiang Zhao, and Hao Zhang. 3d-front: 3d furnished rooms with layouts and semantics. In *2021 IEEE/CVF International Conference on Computer Vision, ICCV 2021, Montreal, QC, Canada, October 10-17, 2021*, pages 10913–10922. IEEE, 2021. 8
- [12] Huan Fu, Rongfei Jia, Lin Gao, Mingming Gong, Binqiang Zhao, Stephen J. Maybank, and Dacheng Tao. 3d-future: 3d furniture shape with texture. *Int. J. Comput. Vis.*, 129(12): 3313–3337, 2021. 6
- [13] Jun Gao, Tianchang Shen, Zian Wang, Wenzheng Chen, Kangxue Yin, Daiqing Li, Or Litany, Zan Gojcic, and Sanja Fidler. GET3D: A generative model of high quality 3d textured shapes learned from images. In *Advances in Neural Information Processing Systems 35: Annual Conference on Neural Information Processing Systems 2022, NeurIPS 2022, New Orleans, LA, USA, November 28 - December 9, 2022*, 2022. 2
- [14] Zekun Hao, David W Romero, Tsung-Yi Lin, and Ming-Yu Liu. Meshtron: High-fidelity, artist-like 3d mesh generation at scale. *arXiv preprint arXiv:2412.09548*, 2024. 3, 4, 5
- [15] Yicong Hong, Kai Zhang, Jiuxiang Gu, Sai Bi, Yang Zhou, Difan Liu, Feng Liu, Kalyan Sunkavalli, Trung Bui, and Hao Tan. LRM: large reconstruction model for single image to 3d. In *The Twelfth International Conference on Learning Representations, ICLR 2024, Vienna, Austria, May 7-11, 2024*. OpenReview.net, 2024. 2
- [16] Yanqin Jiang, Chaohui Yu, Chenjie Cao, Fan Wang, Weiming Hu, and Jin Gao. Animate3d: Animating any 3d model with multi-view video diffusion. In *Advances in Neural Information Processing Systems 38: Annual Conference on Neural Information Processing Systems 2024, NeurIPS 2024, Vancouver, BC, Canada, December 10 - 15, 2024*, 2024. 2
- [17] Heewoo Jun and Alex Nichol. Shap-e: Generating conditional 3d implicit functions. *arXiv preprint arXiv:2305.02463*, 2023. 2
- [18] Bernhard Kerbl, Georgios Kopanas, Thomas Leimkühler, and George Drettakis. 3d gaussian splatting for real-time radiance field rendering. *ACM Trans. Graph.*, 42(4):139:1–139:14, 2023. 2
- [19] Jeonghwan Kim, Yushi Lan, Armando Fortes, Yongwei Chen, and Xingang Pan. Fastmesh: Efficient artistic mesh generation via component decoupling. *arXiv preprint arXiv:2508.19188*, 2025. 6
- [20] Jiahao Li, Hao Tan, Kai Zhang, Zexiang Xu, Fujun Luan, Yinghao Xu, Yicong Hong, Kalyan Sunkavalli, Greg Shakhnarovich, and Sai Bi. Instant3d: Fast text-to-3d with sparse-view generation and large reconstruction model. In *The Twelfth International Conference on Learning Representations, ICLR 2024, Vienna, Austria, May 7-11, 2024*. OpenReview.net, 2024. 2
- [21] Wei Yu Li, Rui Chen, Xuelin Chen, and Ping Tan. Sweetdreamer: Aligning geometric priors in 2d diffusion for consistent text-to-3d. In *The Twelfth International Conference on Learning Representations, ICLR 2024, Vienna, Austria, May 7-11, 2024*. OpenReview.net, 2024. 2
- [22] Wei Yu Li, Jiarui Liu, Hongyu Yan, Rui Chen, Yixun Liang, Xuelin Chen, Ping Tan, and Xiaoxiao Long. Crafts-

- man3d: High-fidelity mesh generation with 3d native generation and interactive geometry refiner. *arXiv preprint arXiv:2405.14979*, 2024. 3
- [23] Yangguang Li, Zi-Xin Zou, Zexiang Liu, Dehu Wang, Yuan Liang, Zhipeng Yu, Xingchao Liu, Yuan-Chen Guo, Ding Liang, Wanli Ouyang, et al. Triposg: High-fidelity 3d shape synthesis using large-scale rectified flow models. *arXiv preprint arXiv:2502.06608*, 2025. 2, 3
- [24] Zhihao Li, Yufei Wang, Heliang Zheng, Yihao Luo, and Bihan Wen. Sparc3d: Sparse representation and construction for high-resolution 3d shapes modeling. *arXiv preprint arXiv:2505.14521*, 2025. 2, 3
- [25] Chen-Hsuan Lin, Jun Gao, Luming Tang, Towaki Takikawa, Xiaohui Zeng, Xun Huang, Karsten Kreis, Sanja Fidler, Ming-Yu Liu, and Tsung-Yi Lin. Magic3d: High-resolution text-to-3d content creation. In *IEEE/CVF Conference on Computer Vision and Pattern Recognition, CVPR 2023, Vancouver, BC, Canada, June 17-24, 2023*, pages 300–309. IEEE, 2023. 2
- [26] Yukang Lin, Haonan Han, Chaoqun Gong, Zunnan Xu, Yachao Zhang, and Xiu Li. Consistent123: One image to highly consistent 3d asset using case-aware diffusion priors. In *Proceedings of the 32nd ACM International Conference on Multimedia, MM 2024, Melbourne, VIC, Australia, 28 October 2024 - 1 November 2024*, pages 6715–6724. ACM, 2024. 2
- [27] Stefan Lionar, Jiabin Liang, and Gim Hee Lee. Treemeshgpt: Artistic mesh generation with autoregressive tree sequencing. In *Proceedings of the Computer Vision and Pattern Recognition Conference*, pages 26608–26617, 2025. 2, 4
- [28] Jian Liu, Chunshi Wang, Song Guo, Haohan Weng, Zhen Zhou, Zhiqi Li, Jiaao Yu, Yiling Zhu, Jing Xu, Biwen Lei, et al. Quadgpt: Native quadrilateral mesh generation with autoregressive models. *arXiv preprint arXiv:2509.21420*, 2025. 2, 3
- [29] Jian Liu, Jing Xu, Song Guo, Jing Li, Jingfeng Guo, Jiaao Yu, Haohan Weng, Biwen Lei, Xianghui Yang, Zhuo Chen, et al. Mesh-rft: Enhancing mesh generation via fine-grained reinforcement fine-tuning. *arXiv preprint arXiv:2505.16761*, 2025. 2, 3
- [30] Minghua Liu, Chao Xu, Haian Jin, Linghao Chen, Mukund Varma T., Zexiang Xu, and Hao Su. One-2-3-45: Any single image to 3d mesh in 45 seconds without per-shape optimization. In *Advances in Neural Information Processing Systems 36: Annual Conference on Neural Information Processing Systems 2023, NeurIPS 2023, New Orleans, LA, USA, December 10 - 16, 2023*, 2023. 2
- [31] Ruoshi Liu, Rundi Wu, Basile Van Hoorick, Pavel Tokmakov, Sergey Zakharov, and Carl Vondrick. Zero-1-to-3: Zero-shot one image to 3d object. In *IEEE/CVF International Conference on Computer Vision, ICCV 2023, Paris, France, October 1-6, 2023*, pages 9264–9275. IEEE, 2023.
- [32] Yuan Liu, Cheng Lin, Zijiao Zeng, Xiaoxiao Long, Lingjie Liu, Taku Komura, and Wenping Wang. Syncdreamer: Generating multiview-consistent images from a single-view image. In *The Twelfth International Conference on Learning Representations, ICLR 2024, Vienna, Austria, May 7-11, 2024*. OpenReview.net, 2024. 2
- [33] Zhen Liu, Yao Feng, Michael J. Black, Derek Nowrouzezahrai, Liam Paull, and Weiyang Liu. Meshdiffusion: Score-based generative 3d mesh modeling. In *The Eleventh International Conference on Learning Representations, ICLR 2023, Kigali, Rwanda, May 1-5, 2023*. OpenReview.net, 2023. 2
- [34] Xiaoxiao Long, Yuan-Chen Guo, Cheng Lin, Yuan Liu, Zhiyang Dou, Lingjie Liu, Yuexin Ma, Song-Hai Zhang, Marc Habermann, Christian Theobalt, and Wenping Wang. Wonder3d: Single image to 3d using cross-domain diffusion. In *IEEE/CVF Conference on Computer Vision and Pattern Recognition, CVPR 2024, Seattle, WA, USA, June 16-22, 2024*, pages 9970–9980. IEEE, 2024. 2
- [35] William E Lorensen and Harvey E Cline. Marching cubes: A high resolution 3d surface construction algorithm. In *Seminal graphics: pioneering efforts that shaped the field*, pages 347–353. 1998. 3
- [36] Zhiyuan Ma, Yuxiang Wei, Yabin Zhang, Xiangyu Zhu, Zhen Lei, and Lei Zhang. Scaledreamer: Scalable text-to-3d synthesis with asynchronous score distillation. In *Computer Vision - ECCV 2024 - 18th European Conference, Milan, Italy, September 29-October 4, 2024, Proceedings, Part VII*, pages 1–19. Springer, 2024. 2
- [37] Ben Mildenhall, Pratul P. Srinivasan, Matthew Tancik, Jonathan T. Barron, Ravi Ramamoorthi, and Ren Ng. Nerf: representing scenes as neural radiance fields for view synthesis. *Commun. ACM*, 65(1):99–106, 2022. 2
- [38] Charlie Nash, Yaroslav Ganin, S. M. Ali Eslami, and Peter W. Battaglia. Polygen: An autoregressive generative model of 3d meshes. In *Proceedings of the 37th International Conference on Machine Learning, ICML 2020, 13-18 July 2020, Virtual Event*, pages 7220–7229. PMLR, 2020. 2, 3
- [39] Alex Nichol, Heewoo Jun, Prafulla Dhariwal, Pamela Mishkin, and Mark Chen. Point-e: A system for generating 3d point clouds from complex prompts. *arXiv preprint arXiv:2212.08751*, 2022. 2
- [40] Ben Poole, Ajay Jain, Jonathan T. Barron, and Ben Mildenhall. Dreamfusion: Text-to-3d using 2d diffusion. In *The Eleventh International Conference on Learning Representations, ICLR 2023, Kigali, Rwanda, May 1-5, 2023*. OpenReview.net, 2023. 2
- [41] Lingteng Qiu, Guanying Chen, Xiaodong Gu, Qi Zuo, Mutian Xu, Yushuang Wu, Weihao Yuan, Zilong Dong, Liefeng Bo, and Xiaoguang Han. Richdreamer: A generalizable normal-depth diffusion model for detail richness in text-to-3d. In *IEEE/CVF Conference on Computer Vision and Pattern Recognition, CVPR 2024, Seattle, WA, USA, June 16-22, 2024*, pages 9914–9925. IEEE, 2024. 2
- [42] Amit Raj, Srinivas Kaza, Ben Poole, Michael Niemeyer, Nataniel Ruiz, Ben Mildenhall, Shiran Zada, Kfir Aberman, Michael Rubinstein, Jonathan T. Barron, Yuanzhen Li, and Varun Jampani. Dreambooth3d: Subject-driven text-to-3d generation. In *IEEE/CVF International Conference on Computer Vision, ICCV 2023, Paris, France, October 1-6, 2023*, pages 2349–2359. IEEE, 2023. 2
- [43] Xuanchi Ren, Jiahui Huang, Xiaohui Zeng, Ken Museth, Sanja Fidler, and Francis Williams. Xcube: Large-scale

- 3d generative modeling using sparse voxel hierarchies. In *IEEE/CVF Conference on Computer Vision and Pattern Recognition, CVPR 2024, Seattle, WA, USA, June 16-22, 2024*, pages 4209–4219. IEEE, 2024. 2
- [44] Jarek Rossignac. Edgebreaker: Connectivity compression for triangle meshes. *IEEE transactions on visualization and computer graphics*, 5(1):47–61, 2002. 3
- [45] Ruoxi Shi, Hansheng Chen, Zhuoyang Zhang, Minghua Liu, Chao Xu, Xinyue Wei, Linghao Chen, Chong Zeng, and Hao Su. Zero123++: a single image to consistent multi-view diffusion base model. *arXiv preprint arXiv:2310.15110*, 2023. 2
- [46] Yichun Shi, Peng Wang, Jianglong Ye, Long Mai, Kejie Li, and Xiao Yang. Mvdream: Multi-view diffusion for 3d generation. In *The Twelfth International Conference on Learning Representations, ICLR 2024, Vienna, Austria, May 7-11, 2024*. OpenReview.net, 2024. 2
- [47] Yawar Siddiqui, Antonio Alliegro, Alexey Artemov, Tatiana Tommasi, Daniele Sirigatti, Vladislav Rosov, Angela Dai, and Matthias Nießner. Meshgpt: Generating triangle meshes with decoder-only transformers. In *IEEE/CVF Conference on Computer Vision and Pattern Recognition, CVPR 2024, Seattle, WA, USA, June 16-22, 2024*, pages 19615–19625. IEEE, 2024. 2, 3, 4
- [48] Yawar Siddiqui, Tom Monnier, Filippos Kokkinos, Mahendra Kariya, Yanir Kleiman, Emilien Garreau, Oran Gafni, Natalia Neverova, Andrea Vedaldi, Roman Shapovalov, and David Novotný. Meta 3d assetgen: Text-to-mesh generation with high-quality geometry, texture, and PBR materials. In *Advances in Neural Information Processing Systems 38: Annual Conference on Neural Information Processing Systems 2024, NeurIPS 2024, Vancouver, BC, Canada, December 10 - 15, 2024*, 2024. 2
- [49] Gaochao Song, Zibo Zhao, Haohan Weng, Jingbo Zeng, Rongfei Jia, and Shenghua Gao. Mesh silksong: Auto-regressive mesh generation as weaving silk. *arXiv preprint arXiv:2507.02477*, 2025. 3, 4, 6
- [50] Stefan Stojanov, Anh Thai, and James M Rehg. Using shape to categorize: Low-shot learning with an explicit shape bias. In *Proceedings of the IEEE/CVF conference on computer vision and pattern recognition*, pages 1798–1808, 2021. 6
- [51] Jingxiang Sun, Bo Zhang, Ruizhi Shao, Lizhen Wang, Wen Liu, Zhenda Xie, and Yebin Liu. Dreamcraft3d: Hierarchical 3d generation with bootstrapped diffusion prior. In *The Twelfth International Conference on Learning Representations, ICLR 2024, Vienna, Austria, May 7-11, 2024*. OpenReview.net, 2024. 2
- [52] Jiaxiang Tang, Zhaoxi Chen, Xiaokang Chen, Tengfei Wang, Gang Zeng, and Ziwei Liu. LGM: large multi-view gaussian model for high-resolution 3d content creation. In *Computer Vision - ECCV 2024 - 18th European Conference, Milan, Italy, September 29-October 4, 2024, Proceedings, Part IV*, pages 1–18. Springer, 2024. 2
- [53] Jiaxiang Tang, Jiawei Ren, Hang Zhou, Ziwei Liu, and Gang Zeng. Dreamgaussian: Generative gaussian splatting for efficient 3d content creation. In *The Twelfth International Conference on Learning Representations, ICLR 2024, Vienna, Austria, May 7-11, 2024*. OpenReview.net, 2024. 2
- [54] Jiaxiang Tang, Zhaoshuo Li, Zekun Hao, Xian Liu, Gang Zeng, Ming-Yu Liu, and Qinsheng Zhang. Edgerunner: Auto-regressive auto-encoder for artistic mesh generation. In *The Thirteenth International Conference on Learning Representations, ICLR 2025, Singapore, April 24-28, 2025*. OpenReview.net, 2025. 2, 3, 4
- [55] Aäron van den Oord, Oriol Vinyals, and Koray Kavukcuoglu. Neural discrete representation learning. In *Advances in Neural Information Processing Systems 30: Annual Conference on Neural Information Processing Systems 2017, December 4-9, 2017, Long Beach, CA, USA*, pages 6306–6315, 2017. 3
- [56] Vikram Voleti, Chun-Han Yao, Mark Boss, Adam Letts, David Pankratz, Dmitry Tochilkin, Christian Laforte, Robin Rombach, and Varun Jampani. SV3D: novel multi-view synthesis and 3d generation from a single image using latent video diffusion. In *Computer Vision - ECCV 2024 - 18th European Conference, Milan, Italy, September 29-October 4, 2024, Proceedings, Part I*, pages 439–457. Springer, 2024. 2
- [57] Haochen Wang, Xiaodan Du, Jiahao Li, Raymond A. Yeh, and Greg Shakhnarovich. Score jacobian chaining: Lifting pretrained 2d diffusion models for 3d generation. In *IEEE/CVF Conference on Computer Vision and Pattern Recognition, CVPR 2023, Vancouver, BC, Canada, June 17-24, 2023*, pages 12619–12629. IEEE, 2023. 2
- [58] Peng Wang and Yichun Shi. Imagedream: Image-prompt multi-view diffusion for 3d generation. *arXiv preprint arXiv:2312.02201*, 2023. 2
- [59] Peng Wang, Hao Tan, Sai Bi, Yinghao Xu, Fujun Luan, Kalyan Sunkavalli, Wenping Wang, Zexiang Xu, and Kai Zhang. PF-LRM: pose-free large reconstruction model for joint pose and shape prediction. In *The Twelfth International Conference on Learning Representations, ICLR 2024, Vienna, Austria, May 7-11, 2024*. OpenReview.net, 2024. 2
- [60] Xinzhou Wang, Yikai Wang, Junliang Ye, Fuchun Sun, Zhengyi Wang, Ling Wang, Pengkun Liu, Kai Sun, Xintong Wang, Wende Xie, Fangfu Liu, and Bin He. Animatable-dreamer: Text-guided non-rigid 3d model generation and reconstruction with canonical score distillation. In *Computer Vision - ECCV 2024 - 18th European Conference, Milan, Italy, September 29-October 4, 2024, Proceedings, Part XXV*, pages 321–339. Springer, 2024. 2
- [61] Zhengyi Wang, Cheng Lu, Yikai Wang, Fan Bao, Chongxuan Li, Hang Su, and Jun Zhu. Prolificdreamer: High-fidelity and diverse text-to-3d generation with variational score distillation. In *Advances in Neural Information Processing Systems 36: Annual Conference on Neural Information Processing Systems 2023, NeurIPS 2023, New Orleans, LA, USA, December 10 - 16, 2023*, 2023. 2
- [62] Zhengyi Wang, Jonathan Lorraine, Yikai Wang, Hang Su, Jun Zhu, Sanja Fidler, and Xiaohui Zeng. Llama-mesh: Unifying 3d mesh generation with language models. *CoRR*, abs/2411.09595, 2024. 3
- [63] Zhengyi Wang, Yikai Wang, Yifei Chen, Chendong Xiang, Shuo Chen, Dajiang Yu, Chongxuan Li, Hang Su, and Jun Zhu. CRM: single image to 3d textured mesh with convolutional reconstruction model. In *Computer Vision - ECCV 2024 - 18th European Conference, Milan, Italy, September*

- 29-October 4, 2024, *Proceedings, Part XXXI*, pages 57–74. Springer, 2024. 2
- [64] Haohan Weng, Yikai Wang, Tong Zhang, C. L. Philip Chen, and Jun Zhu. Pivotmesh: Generic 3d mesh generation via pivot vertices guidance. In *The Thirteenth International Conference on Learning Representations, ICLR 2025, Singapore, April 24-28, 2025*. OpenReview.net, 2025. 3
- [65] Haohan Weng, Zibo Zhao, Biwen Lei, Xianghui Yang, Jian Liu, Zeqiang Lai, Zhuo Chen, Yuhong Liu, Jie Jiang, Chunchao Guo, Tong Zhang, Shenghua Gao, and C. L. Philip Chen. Scaling mesh generation via compressive tokenization. In *IEEE/CVF Conference on Computer Vision and Pattern Recognition, CVPR 2025, Nashville, TN, USA, June 11-15, 2025*, pages 11093–11103. Computer Vision Foundation / IEEE, 2025. 2, 3, 4, 6
- [66] Kailu Wu, Fangfu Liu, Zhihan Cai, Runjie Yan, Hanyang Wang, Yating Hu, Yueqi Duan, and Kaisheng Ma. Unique3d: High-quality and efficient 3d mesh generation from a single image. In *Advances in Neural Information Processing Systems 38: Annual Conference on Neural Information Processing Systems 2024, NeurIPS 2024, Vancouver, BC, Canada, December 10 - 15, 2024*, 2024. 2
- [67] Shuang Wu, Youtian Lin, Yifei Zeng, Feihu Zhang, Jingxi Xu, Philip Torr, Xun Cao, and Yao Yao. Direct3d: Scalable image-to-3d generation via 3d latent diffusion transformer. In *Advances in Neural Information Processing Systems 38: Annual Conference on Neural Information Processing Systems 2024, NeurIPS 2024, Vancouver, BC, Canada, December 10 - 15, 2024*, 2024. 3
- [68] Shuang Wu, Youtian Lin, Feihu Zhang, Yifei Zeng, Yikang Yang, Yajie Bao, Jiachen Qian, Siyu Zhu, Xun Cao, Philip Torr, et al. Direct3d-s2: Gigascale 3d generation made easy with spatial sparse attention. *arXiv preprint arXiv:2505.17412*, 2025. 2
- [69] Jianfeng Xiang, Zelong Lv, Sicheng Xu, Yu Deng, Ruicheng Wang, Bowen Zhang, Dong Chen, Xin Tong, and Jiaolong Yang. Structured 3d latents for scalable and versatile 3d generation. In *IEEE/CVF Conference on Computer Vision and Pattern Recognition, CVPR 2025, Nashville, TN, USA, June 11-15, 2025*, pages 21469–21480. Computer Vision Foundation / IEEE, 2025. 2, 3, 6, 7
- [70] Yinghao Xu, Zifan Shi, Yifan Wang, Hansheng Chen, Ceyuan Yang, Sida Peng, Yujun Shen, and Gordon Wetzstein. GRM: large gaussian reconstruction model for efficient 3d reconstruction and generation. In *Computer Vision - ECCV 2024 - 18th European Conference, Milan, Italy, September 29-October 4, 2024, Proceedings, Part XV*, pages 1–20. Springer, 2024. 2
- [71] Yinghao Xu, Hao Tan, Fujun Luan, Sai Bi, Peng Wang, Jiahao Li, Zifan Shi, Kalyan Sunkavalli, Gordon Wetzstein, Zexiang Xu, and Kai Zhang. DMV3D: denoising multi-view diffusion using 3d large reconstruction model. In *The Twelfth International Conference on Learning Representations, ICLR 2024, Vienna, Austria, May 7-11, 2024*. OpenReview.net, 2024. 2
- [72] Haibo Yang, Yang Chen, Yingwei Pan, Ting Yao, Zhineng Chen, Chong-Wah Ngo, and Tao Mei. Hi3d: Pursuing high-resolution image-to-3d generation with video diffusion models. In *Proceedings of the 32nd ACM International Conference on Multimedia, MM 2024, Melbourne, VIC, Australia, 28 October 2024 - 1 November 2024*, pages 6870–6879. ACM, 2024. 2
- [73] Chongjie Ye, Yushuang Wu, Ziteng Lu, Jiahao Chang, Xiaoyang Guo, Jiaqing Zhou, Hao Zhao, and Xiaoguang Han. Hi3dgen: High-fidelity 3d geometry generation from images via normal bridging. 3
- [74] Junliang Ye, Fangfu Liu, Qixiu Li, Zhengyi Wang, Yikai Wang, Xinzhou Wang, Yueqi Duan, and Jun Zhu. Dream-ward: Text-to-3d generation with human preference. In *Computer Vision - ECCV 2024 - 18th European Conference, Milan, Italy, September 29-October 4, 2024, Proceedings, Part LXX*, pages 259–276. Springer, 2024. 2
- [75] Taoran Yi, Jiemin Fang, Junjie Wang, Guanjun Wu, Lingxi Xie, Xiaopeng Zhang, Wenyu Liu, Qi Tian, and Xinggang Wang. Gaussiandreamer: Fast generation from text to 3d gaussians by bridging 2d and 3d diffusion models. In *IEEE/CVF Conference on Computer Vision and Pattern Recognition, CVPR 2024, Seattle, WA, USA, June 16-22, 2024*, pages 6796–6807. IEEE, 2024. 2
- [76] Jingyang Yuan, Huazuo Gao, Damai Dai, Junyu Luo, Liang Zhao, Zhengyan Zhang, Zhenda Xie, Yuxing Wei, Lean Wang, Zhiping Xiao, Yuqing Wang, Chong Ruan, Ming Zhang, Wenfeng Liang, and Wangding Zeng. Native sparse attention: Hardware-aligned and natively trainable sparse attention. In *Proceedings of the 63rd Annual Meeting of the Association for Computational Linguistics (Volume 1: Long Papers), ACL 2025, Vienna, Austria, July 27 - August 1, 2025*, pages 23078–23097. Association for Computational Linguistics, 2025. 5
- [77] Biao Zhang, Jiapeng Tang, Matthias Nießner, and Peter Wonka. 3dshape2vecset: A 3d shape representation for neural fields and generative diffusion models. *ACM Trans. Graph.*, 42(4):92:1–92:16, 2023. 2
- [78] Chubin Zhang, Hongliang Song, Yi Wei, Chen Yu, Jiwen Lu, and Yansong Tang. Geolrm: Geometry-aware large reconstruction model for high-quality 3d gaussian generation. In *Advances in Neural Information Processing Systems 38: Annual Conference on Neural Information Processing Systems 2024, NeurIPS 2024, Vancouver, BC, Canada, December 10 - 15, 2024*, 2024. 2
- [79] Kai Zhang, Sai Bi, Hao Tan, Yuanbo Xiangli, Nanxuan Zhao, Kalyan Sunkavalli, and Zexiang Xu. GS-LRM: large reconstruction model for 3d gaussian splatting. In *Computer Vision - ECCV 2024 - 18th European Conference, Milan, Italy, September 29-October 4, 2024, Proceedings, Part XXII*, pages 1–19. Springer, 2024. 2
- [80] Longwen Zhang, Ziyu Wang, Qixuan Zhang, Qiwei Qiu, Anqi Pang, Haoran Jiang, Wei Yang, Lan Xu, and Jingyi Yu. CLAY: A controllable large-scale generative model for creating high-quality 3d assets. *ACM Trans. Graph.*, 43(4): 120:1–120:20, 2024. 2
- [81] Ruowen Zhao, Zhengyi Wang, Yikai Wang, Zihan Zhou, and Jun Zhu. Flexidreamer: single image-to-3d generation with flexicubes. *arXiv preprint arXiv:2404.00987*, 2024. 2
- [82] Ruowen Zhao, Junliang Ye, Zhengyi Wang, Guangce Liu, Yiwen Chen, Yikai Wang, and Jun Zhu. Deepmesh: Auto-

- regressive artist-mesh creation with reinforcement learning. In *Proceedings of the IEEE/CVF International Conference on Computer Vision*, pages 10612–10623, 2025. [2](#), [3](#), [4](#), [5](#), [6](#)
- [83] Zibo Zhao, Zeqiang Lai, Qingxiang Lin, Yunfei Zhao, Haolin Liu, Shuhui Yang, Yifei Feng, Mingxin Yang, Sheng Zhang, Xianghui Yang, et al. Hunyuan3d 2.0: Scaling diffusion models for high resolution textured 3d assets generation. *arXiv preprint arXiv:2501.12202*, 2025. [2](#), [3](#)
- [84] Chen Ziwen, Hao Tan, Kai Zhang, Sai Bi, Fujun Luan, Yicong Hong, Li Fuxin, and Zexiang Xu. Long-lrm: Long-sequence large reconstruction model for wide-coverage gaussian splats. In *Proceedings of the IEEE/CVF International Conference on Computer Vision*, pages 4349–4359, 2025. [2](#)
- [85] Zi-Xin Zou, Zhipeng Yu, Yuan-Chen Guo, Yangguang Li, Ding Liang, Yan-Pei Cao, and Song-Hai Zhang. Triplane meets gaussian splatting: Fast and generalizable single-view 3d reconstruction with transformers. In *IEEE/CVF Conference on Computer Vision and Pattern Recognition, CVPR 2024, Seattle, WA, USA, June 16-22, 2024*, pages 10324–10335. IEEE, 2024. [2](#)
- [86] Qi Zuo, Xiaodong Gu, Yuan Dong, Zhengyi Zhao, Weihao Yuan, Lingteng Qiu, Liefeng Bo, and Zilong Dong. High-fidelity 3d textured shapes generation by sparse encoding and adversarial decoding. In *European Conference on Computer Vision*, 2024. [6](#)

MeshRipple: Structured Autoregressive Generation of Artist-Meshes

Supplementary Material

A. Ripple Tokenization Algorithm

Algorithm 1: Ripple Tokenization

```

Input      : Mesh  $\mathcal{M}$ 
Preprocess:  $\mathcal{M} \rightarrow$  Half Edges  $\mathbf{H} = \{\mathbf{h}_i\}_N$ 
Output    : Sequence  $\mathcal{S}$ , Root Index  $\mathbf{R}$ 
Data: FIFO Frontier Queue  $\mathcal{B}$ 

 $\mathcal{S}.$ append(BOS);
for HalfEdge  $\mathbf{h}$  in  $\mathbf{H}$ :
  if  $\mathbf{h}.$ face.vis:
    continue;
   $\mathbf{h}.$ face.vis = true;
   $\mathcal{B}.$ enqueue( $\mathbf{h}$ );
   $\mathcal{S}.$ append(N);
  AddFace ( $\mathcal{S}$ ,  $\mathbf{h}$ );
  while  $\mathcal{B}$  is not empty:
     $\mathbf{h} = \mathcal{B}.$ dequeue();
    for HalfEdge  $\mathbf{h}_o$  in [ $\mathbf{h}.$ p.o;  $\mathbf{h}.$ n.o;  $\mathbf{h}.$ o]:
      if not  $\mathbf{h}_o.$ face.vis:
         $\mathbf{h}_o.$ face.vis = true;
        AddFace ( $\mathcal{S}$ ,  $\mathbf{h}_o$ );
        RecordRoot ( $\mathbf{R}$ ,  $\mathbf{h}$ ,  $\mathbf{h}_o$ );
         $\mathcal{B}.$ enqueue( $\mathbf{h}_o$ );
  Project  $\mathcal{S}$  to vertex coordinates
  Output  $\mathcal{S}$ ,  $\mathbf{R}$ 
  
```

In this section, we elaborate on the proposed Ripple Tokenization. We begin by preprocessing the input mesh: vertices are quantized into discrete bins (set to 256 in our experiments), duplicated vertices are merged, and degenerate faces are removed. This yields a sanitized mesh $\mathcal{M} = \{\mathcal{F}, \mathcal{V}\}$, where each face $\mathbf{F}_i \in \mathcal{F}$ is defined as $\mathbf{F}_i = [\mathbf{a}_0^i, \mathbf{a}_1^i, \mathbf{a}_2^i]$, containing the indices of the vertices forming the face. To establish a deterministic traversal order, we sort all faces lexicographically based on their vertex coordinates (specifically using z - y - x ordering). Subsequently, we construct a half-edge data structure for the mesh, respecting the orientation defined by the face normals. The tokenization process employs a breadth-first traversal initialized at the first half-edge of the lexicographically first face, \mathbf{F}_0 . During each iteration, a half-edge \mathbf{h} is dequeued, and we sequentially access the twin half-edges of its predecessor ($\mathbf{h}.$ p), its successor ($\mathbf{h}.$ n), and the half-edge itself (\mathbf{h}). This sequence strictly defines the traversal priority for the neighbors of any given face \mathbf{F}_i . To prevent cy-

cles and redundancy, we maintain a binary visitation state, *vis*, for each face. When a neighboring face is accessed via a twin half-edge, we check its state; if it has not yet been visited, we mark *vis* as true and add the corresponding half-edge to the queue. This propagation continues until all reachable half-edges in the connected component have been processed.

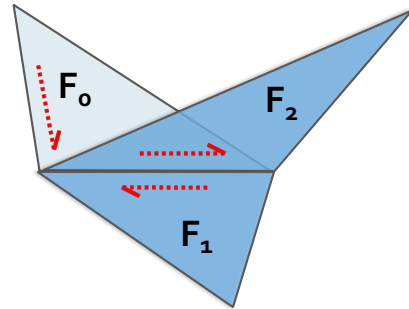


Figure 8. **Illustration of Non-Manifold Traversal Strategy.** Direct traversal between F_0 and F_2 is inhibited because their incident half-edges are co-directional. The algorithm resolves this by extending traversal through the intermediate face F_1 , maintaining normal vector consistency.

Non-manifoldness. To ensure consistent surface orientation, our algorithm restricts traversal across non-manifold edges to incident half-edges with opposite orientations. Consequently, traversal is explicitly inhibited when an adjacent half-edge is co-directional with the current half-edge. As illustrated in Figure 8, although faces \mathbf{F}_0 and \mathbf{F}_2 share identical normal vectors, the co-directionality of their shared boundary prevents direct propagation between them. However, structural connectivity allows for indirect traversal. In the example shown, the algorithm successfully propagates from \mathbf{F}_0 to \mathbf{F}_1 , provided their interface satisfies the orientation constraint (opposite half-edges). From \mathbf{F}_1 , the traversal can subsequently extend to \mathbf{F}_2 . Crucially, in scenarios where a face is effectively isolated by co-directional half-edges on all sides—indicating an irresolvable conflict in face normals—we interpret this as a topological discontinuity and segregate the regions into separate connected components.

Disconnected Components. For each independent connected component, the starting face lacks a preceding frontier face. Consequently, we assign a special token **N** to explicitly mark the initiation of a new component, as illustrated in Figure 9.

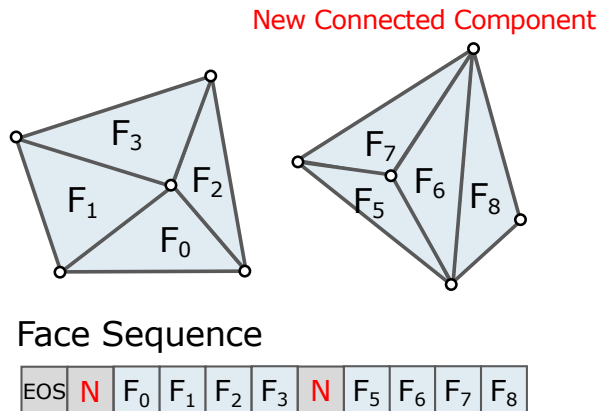


Figure 9. **Initialization of Disconnected Components.** When initiating traversal for a topologically disjoint component, the starting face lacks a preceding frontier face. A special identifier N is used to explicitly mark this boundary.

B. More Implementation Details

B.1. Filtering Training Data

Table 5. **Model Architecture Hyperparameters.**

	Small scale	Large scale
Parameter count	500 M	800M
Batch Size	8	4
Hourglass	4,4,9	4,4,9
Heads	10	16
d_{model}	768	1024
d_{FFN}	3072	4096
Learning rate	$1e - 4$	$1e - 4$
LR scheduler	Cosine	Cosine
Weight decay	0.1	0.1
Gradient Clip	1.0	1.0

B.2. More Training Details

The significant variance in data quality across collected datasets poses a challenge for robust model training. To address this, we implement a strict filtering pipeline based on geometric topology and quantization artifacts.

Geometric and Topological Filtering. We discard meshes with face counts outside the range $[500, 20k]$, vertex-to-face ratios > 0.8 , or where narrow faces (minimum angle $< 5^\circ$) exceed 20% of the total. To ensure topological simplicity, we exclude meshes exceeding a maximum BFS displacement of 100, a boundary length of 500, or 20 connected components. The component count is determined after pruning small clusters (< 10 faces) located within a normalized distance of 0.05 from valid components.

Vertex Merge Filtering. To mitigate artifacts from discrete vertex merging, we filter meshes where the vertex count drops by $> 50\%$, or where newly introduced self-intersecting or overlapping faces exceed 10%. Self-intersections are detected via `trimesh`, while overlapping faces are identified by grouping coplanar faces and verifying candidates via the Separating Axis Theorem (SAT).

We implemented two variants of MeshRipple: a small-scale model and a large-scale model. The detailed architectural specifications are presented in Table 5. It is worth noting that the reported parameter counts include the parameters of Michelangelo encoder. Furthermore, to optimize GPU memory usage, we utilized `bfloat16` (bf16) precision and FlashAttention.

Furthermore, we employ point cloud noise injection, rotation, and scaling for data augmentation. Specifically, during point cloud sampling, Gaussian noise is added to the vertex coordinates with a probability of 0.5. For rotation, the mesh is set to perform rotational augmentation around the z -axis, with each unit being 30° , covering a total of 360° . Finally, for scaling, we uniformly sample a scaling factor from the range $[0.75, 1.25]$ for each axis.

C. More Ablation Study

Table 6. **Ablation study on the truncation window size.** Metrics are evaluated on 160 dense meshes.

Window Size	CD (\downarrow)	HD (\downarrow)	NC (\uparrow)
1k	0.051948	0.109130	0.796585
2k	0.050651	0.104539	0.798088

Truncation Window Size. We conduct an ablation study on the truncation window size, comparing 1k and 2k, on a dataset of 100k samples. The evaluation is performed on 160 dense meshes, with results presented in Table 6.

Resources w/o NSCA. Table 7 compares the computational resource consumption with and without NSCA across various configurations. We have noticed the advantages of NSCA in terms of time and GPU memory resource consumption in long sequences, which can help us extend MeshRipple to longer window and longer mesh face amount.

D. More Results

We present additional qualitative comparisons with BPT and DeepMesh in Figure 10, where the face count for each mesh is explicitly annotated. Furthermore, extended results for point cloud-conditioned generation are illustrated in Figure 11 and Figure 12. Finally, Figure 13, Figure 14, Figure 15 and Figure 16 displays high-resolution visualiza-

Table 7. **GPU memory (GB) and runtime (s) comparison w/o NSCA on a single A800 GPU.** Each configuration is evaluated and averaged over 128 iterations. Context and window sizes are measured in number of faces.

Total Faces	Window	NSCA		w/o NSCA	
		Time	Mem	Time	Mem
5K	1K	0.253	24.65	0.180	27.68
5K	2K	0.391	29.94	0.335	33.68
5K	5K	1.199	47.85	1.156	53.59
10K	1K	0.252	24.72	0.199	28.50
10K	2K	0.393	30.01	0.362	35.17
10K	5K	1.194	47.91	1.207	57.13
20K	1K	0.254	24.86	0.244	30.16
20K	2K	0.398	30.16	0.419	38.15
20K	5K	1.200	48.05	OOM	
50K	1K	0.265	25.34	0.426	35.09
50K	2K	0.420	30.61	0.636	47.19
50K	5K	1.229	48.46	OOM	
100K	1K	0.300	26.13	0.726	43.35
100K	2K	0.458	31.42	0.984	62.26
100K	5K	1.275	49.19	OOM	

tions to facilitate a detailed inspection of the geometric fine structures.

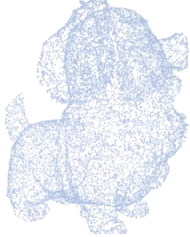
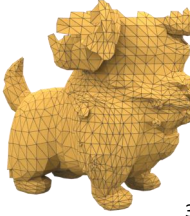
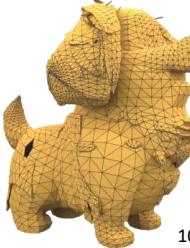
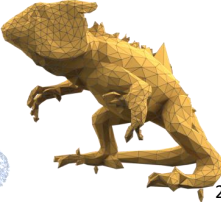
Origin Mesh	Point Cloud	BPT	DeepMesh	Ours
		 1915	 13454	 11803
		 3819	 10211	 12359
		 2898	 23152	 7550
		 4733	 18655	 13677
		 3740	 18568	 14171
		 2457	 6703	 7186

Figure 10. More comparisons between MeshRipple and the SOTAs.

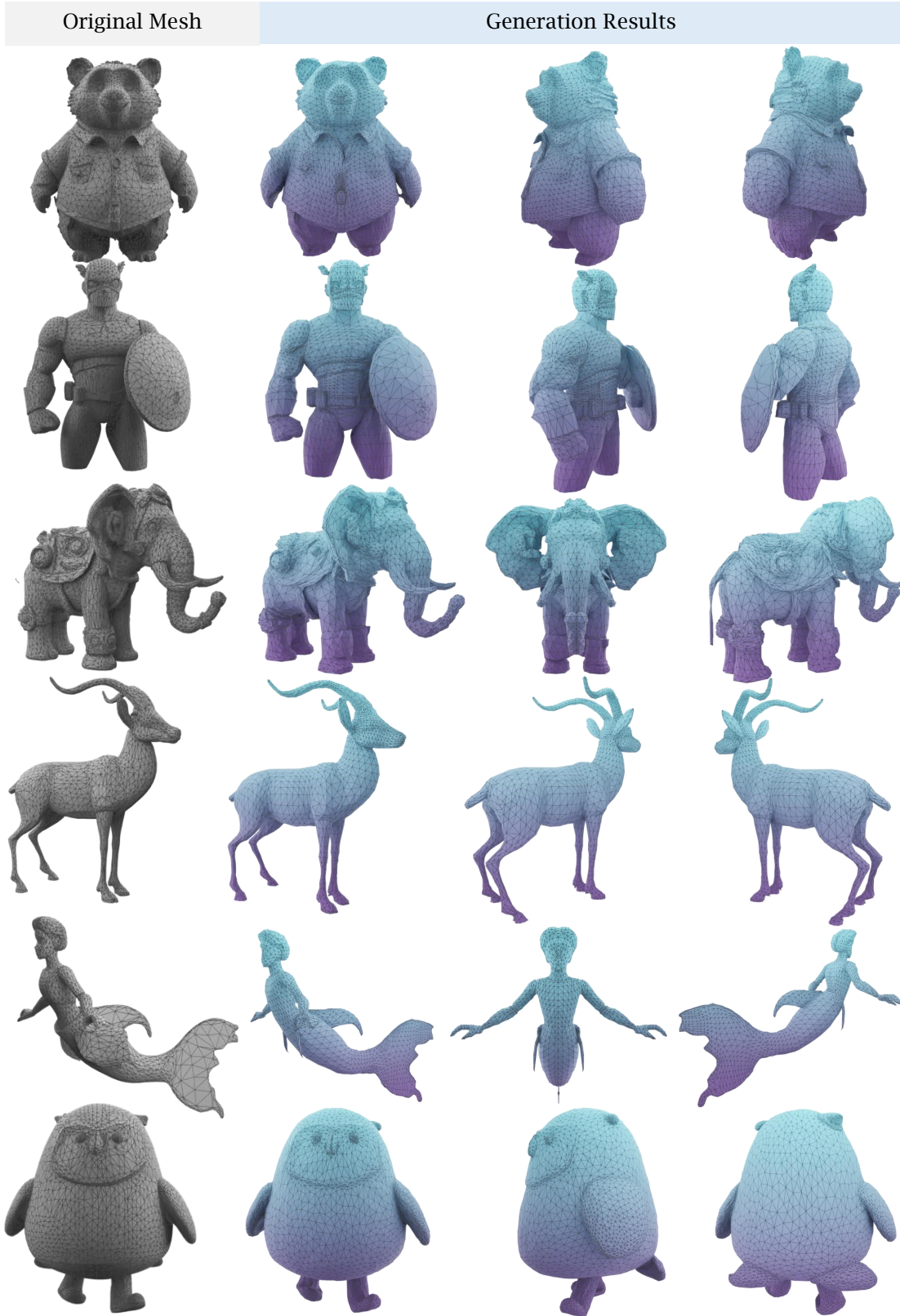


Figure 11. More results generated by MeshRipple.

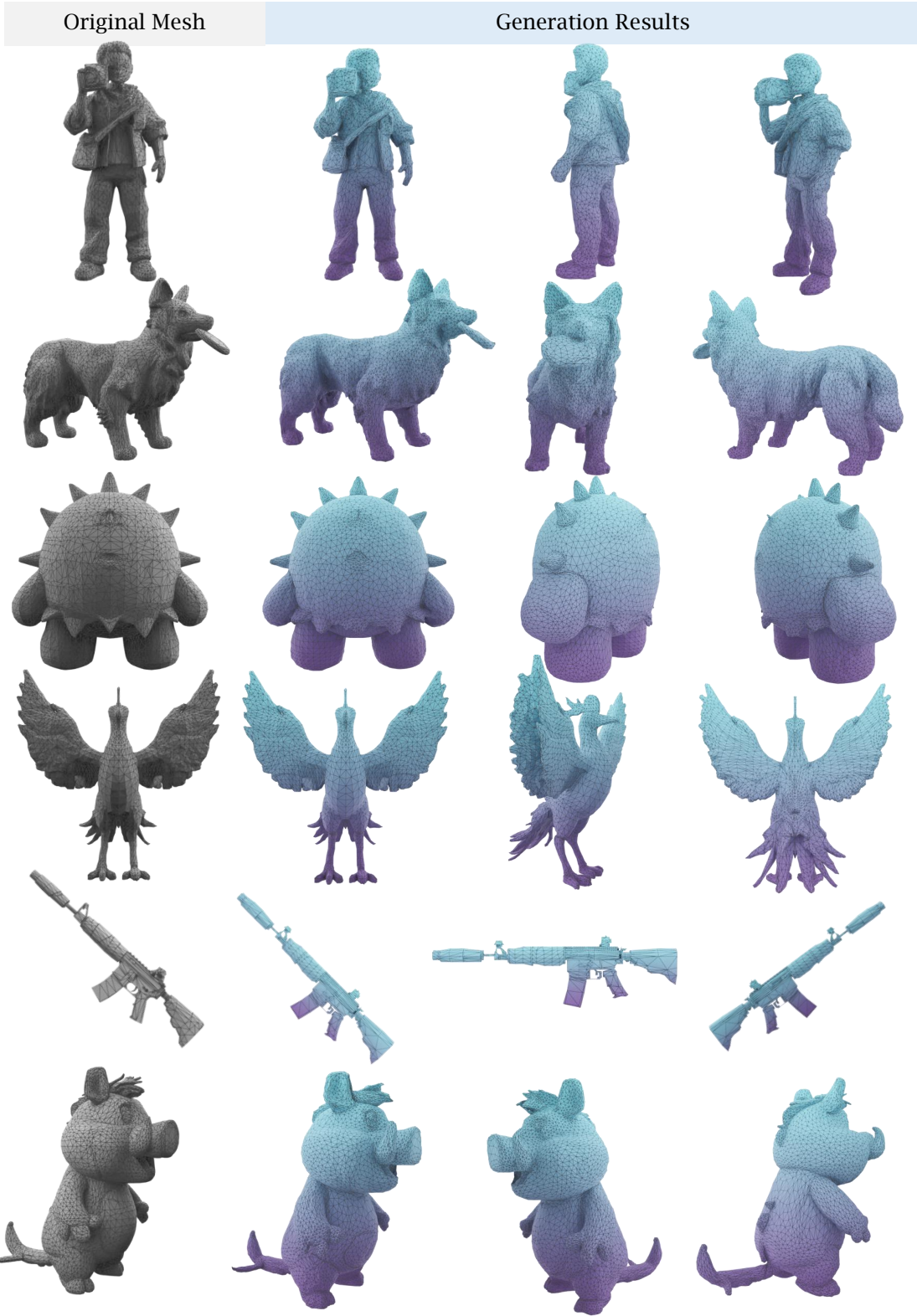


Figure 12. More results generated by MeshRipple.

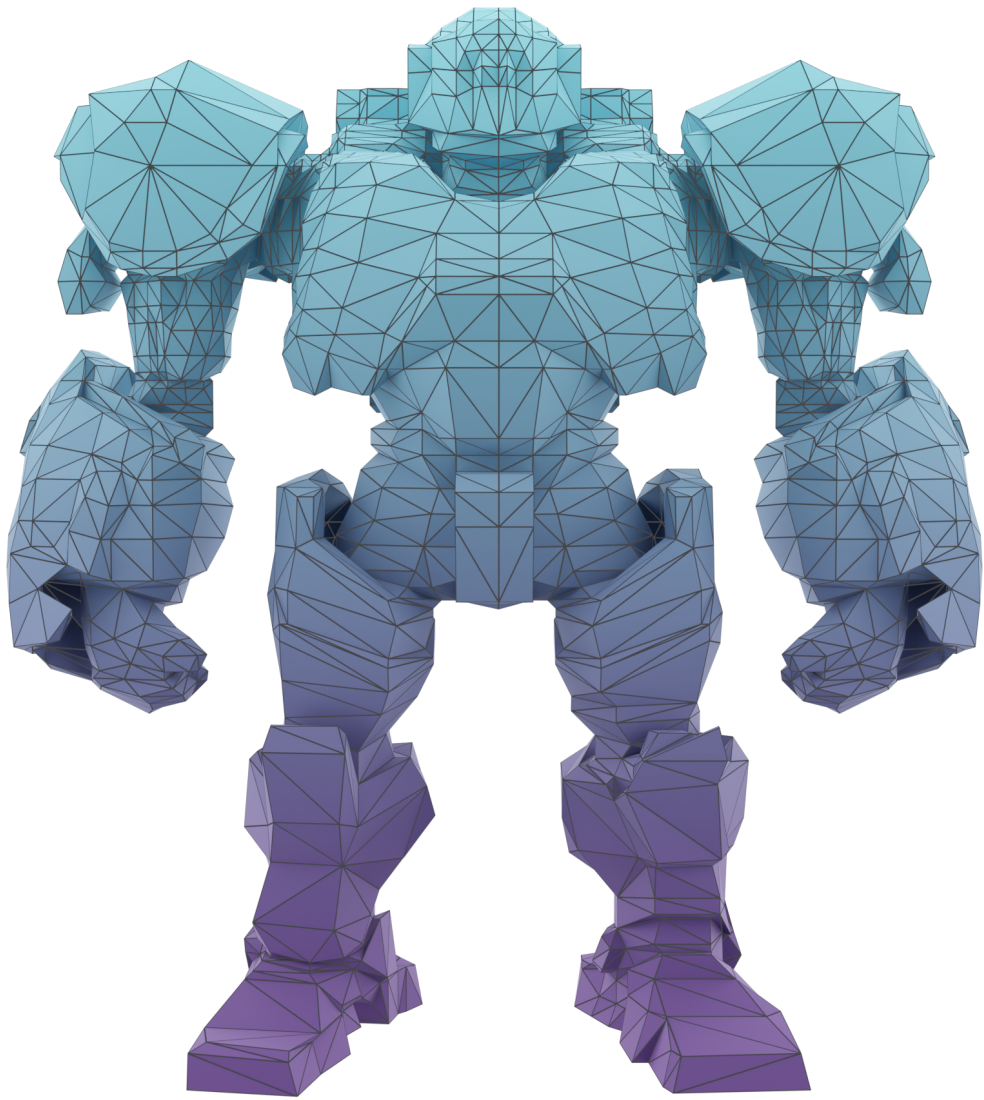


Figure 13. **High-fidelity visualizations of generated meshes.**

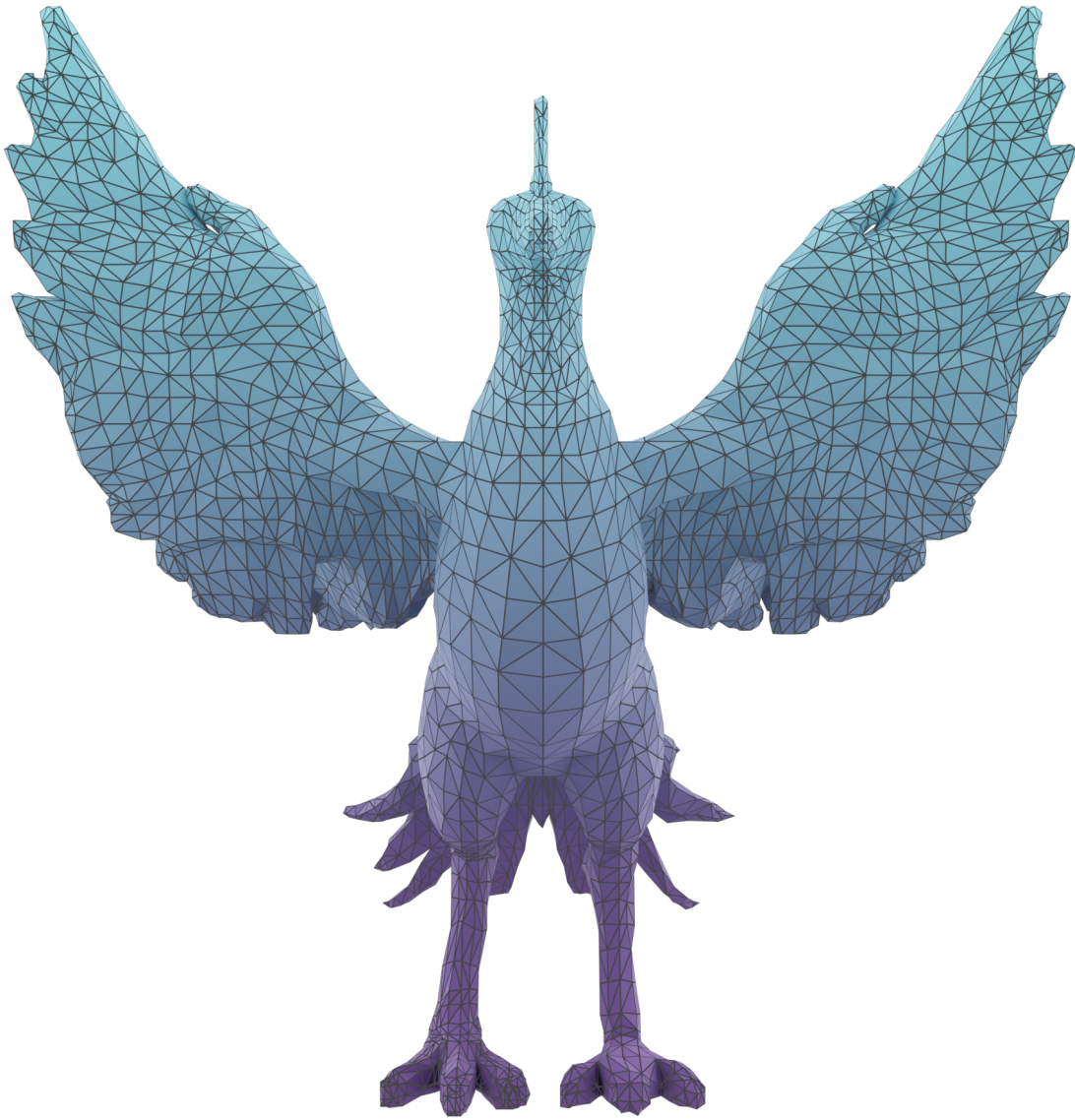


Figure 14. **High-fidelity visualizations of generated meshes.**

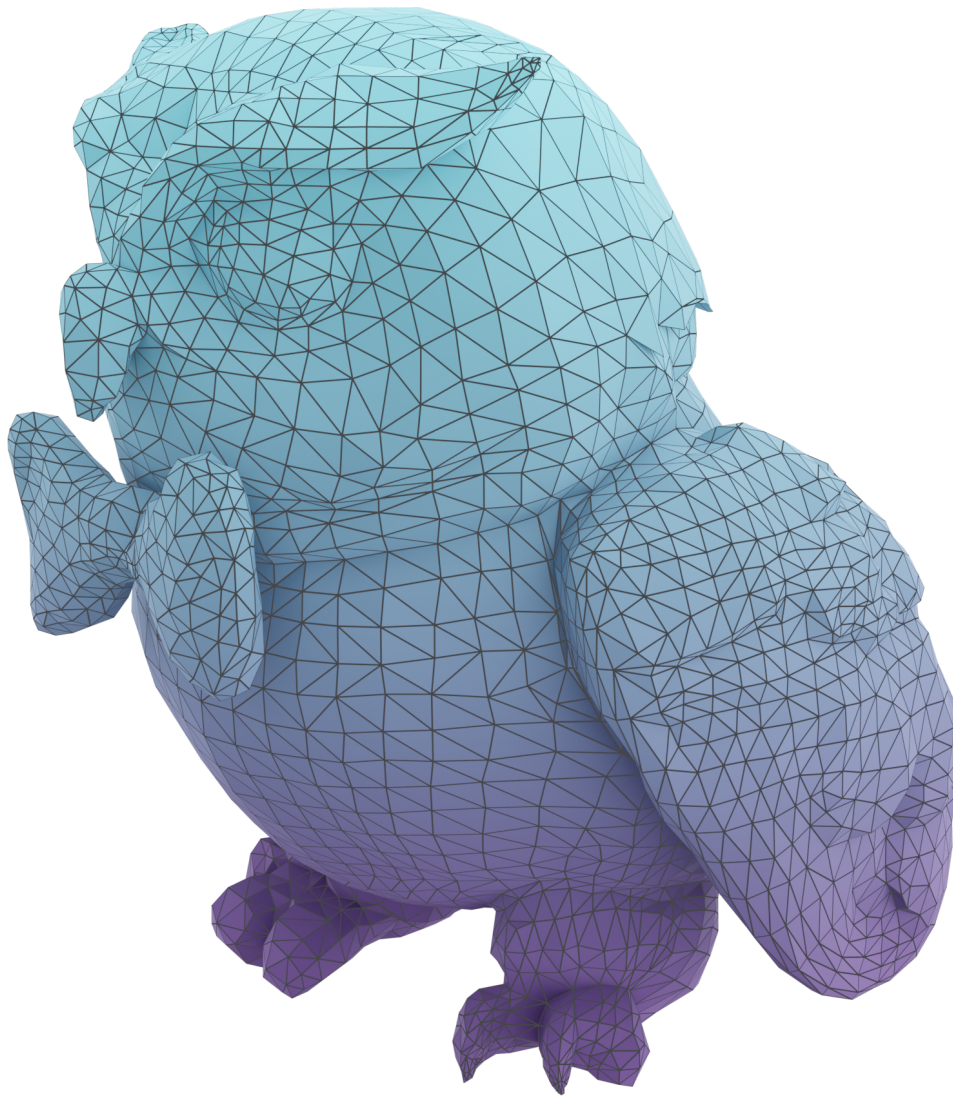


Figure 15. **High-fidelity visualizations of generated meshes.**

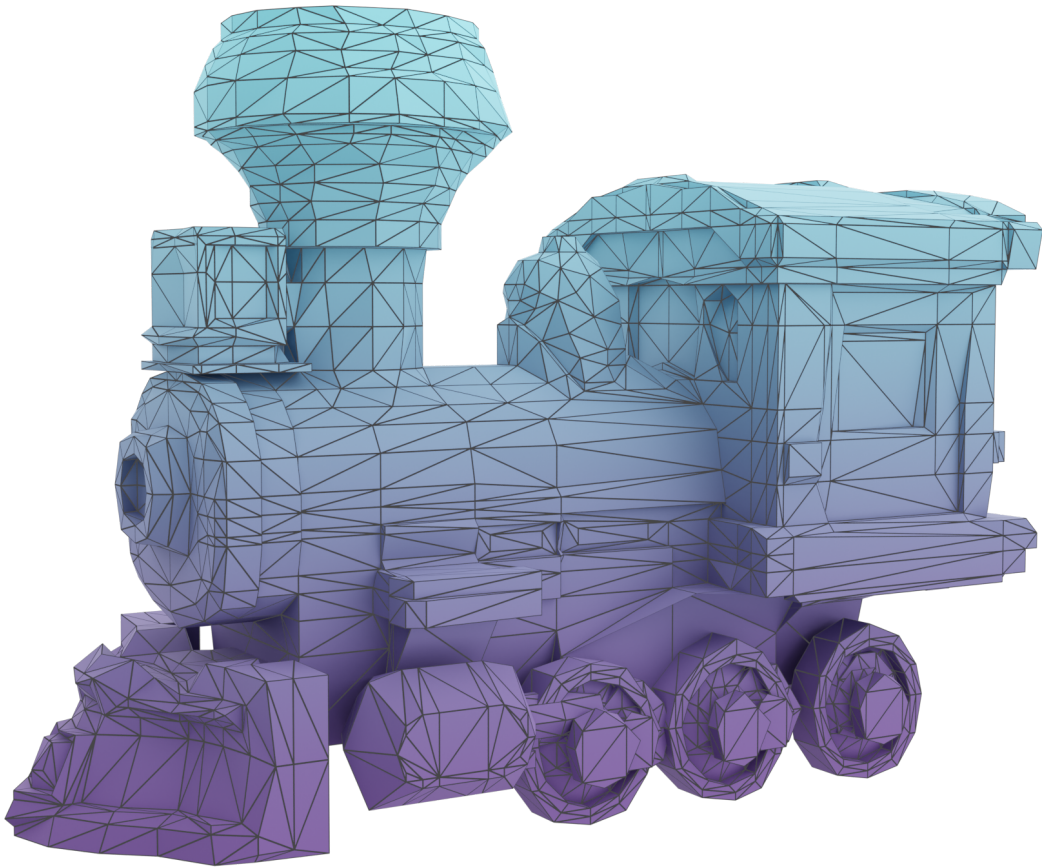


Figure 16. **High-fidelity visualizations of generated meshes.**